Front. Optoelectron. China 2010, 3(3): 232–240
DOI 10.1007/s12200-010-0101-1

RESEARCH ARTICLE

Circuit modeling of quantum dot semiconductor optical amplifier

Yi YU, Lirong HUANG (✉), Meng XIONG, Dexiu HUANG

College of Optoelectronic Science and Engineering, Wuhan National Laboratory for Optoelectronics, Huazhong University of Science and Technology, Wuhan 430074, China

© Higher Education Press and Springer-Verlag Berlin Heidelberg 2010

Abstract A circuit model of a quantum dot semiconductor optical amplifier is proposed by employing standard rate equations. Using this model, the saturation property and dynamic performance of the quantum dot semiconductor optical amplifier are analyzed by PSPICE simulation. We also investigate wavelength conversion based on cross-gain modulation for the quantum dot semiconductor optical amplifier. The corresponding results are in agreement with the previous published works.

Keywords quantum dot, semiconductor optical amplifier, circuit model, cross gain modulation, wavelength conversion

1 Introduction

Quantum dot (QD) structures have attracted considerable attention especially in the field of optical communications, and it has already demonstrated improved performances in many respects such as higher differential gain, faster gain recovery, lower noise factor and better temperature stability compared with bulk and quantum well (QW) structures [1–4]. Because of these advantages, the quantum dot semiconductor optical amplifier (QD-SOA) has received extensive studies in the last decade [5–10]. Notable interest in ultrafast carrier dynamics has focused on QD lasers and optical amplifiers for applications in high speed systems [11,12]. However, intensive and complicated computational programs are needed to perform the simulations, and device-level programs for QD-SOA are not suitable for sophisticated optoelectronic system designs.

Considering the simulation efficiency of the existing and well-developed circuit simulators such as PSPICE, circuit models of bulk, QW and QD lasers have been developed [13–17]. Very recently, Maram proposed a circuit model of QD-SOA [18]. In this paper, we propose a new equivalent circuit model for QD-SOA with a better convergence property, and apply this circuit model to analyze the saturation property and dynamic performance of QD-SOA. Furthermore, based on cross-gain modulation (XGM), we use the circuit model of QD-SOA to investigate wavelength conversion.

This paper is organized as follows. Based on the basic theoretical model, a sub-circuit model implementation of QD-SOA is described and the corresponding simulation results are discussed in Sect. 2. In Sect. 3, we use our presented circuit model to analyze wavelength conversion based on XGM. Finally, a brief conclusion is given in Sect. 4.

2 Theoretical model of QD-SOA

2.1 Basic model of QD-SOA based on standard rate equations

A comprehensive energy band diagram of QD-SOA is presented in our study given in Fig. 1. It includes the presence of the separate confinement heterostructure (SCH) [10,19], the wetting layer (WL) [10,19–21], the discrete excited state (ES) and the ground state (GS) [19–21].

The carriers are injected into the SCH layer with a rate of $I/(qV)$, where I is the injection current, q is the electron charge, V is the volume of the active region of QD-SOA. WL acts as a carrier reservoir, and relaxes the carriers into the ES level of QD, then the GS level of QD. The associated time constants are the carrier diffusion time from SCH to WL (τ_{sw}), carrier escape time from WL to SCH (τ_{ws}), carrier relaxation time from WL to ES (τ_{we}), escape time from ES to WL (τ_{ew}), relaxation time from ES

Received April 2, 2010; accepted April 30, 2010

E-mail: hlr5649@163.com

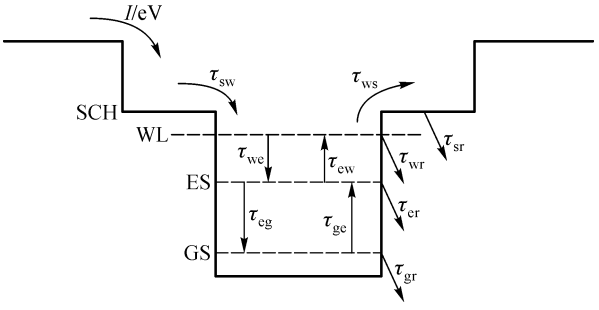


Fig. 1 Schematic energy band diagram of QD-SOA

to GS (τ_{eg}), escape time from GS to ES (τ_{ge}), carrier recombination time in SCH (τ_{sr}), recombination time in WL (τ_{wr}), and recombination time in ES (τ_{er}) and GS (τ_{gr}), respectively. Because the carrier exchange between WL and ES is especially strong, the direct carrier transfer between spatially localized QDs can be neglected [21]. The resulting rate equation system is as follows:

$$\frac{dN_s}{dt} = \frac{I}{qV} - \frac{N_s}{\tau_{sw}} - \frac{N_s}{\tau_{sr}} + \frac{N_w}{\tau_{ws}}, \tag{1}$$

$$\frac{dN_w}{dt} = \frac{N_s}{\tau_{sw}} - \frac{N_w}{\tau_{ws}} + \frac{N_e}{\tau_{ew}} - \frac{N_w}{\tau_{we}}\left(1 - \frac{N_e}{N_{DE}}\right) - \frac{N_w}{\tau_{wr}}, \tag{2}$$

$$\frac{dN_e}{dt} = \frac{N_w}{\tau_{we}}\left(1 - \frac{N_e}{N_{DE}}\right) - \frac{N_e}{\tau_{ew}} + \frac{N_g}{\tau_{ge}}\left(1 - \frac{N_e}{N_{DE}}\right) - \frac{N_e}{\tau_{eg}}\left(1 - \frac{N_g}{N_{DG}}\right) - \frac{N_e}{\tau_{er}} - \Gamma v_g \frac{g_E}{1 + \varepsilon S_{ave}} S_{ave}, \tag{3}$$

$$\frac{dN_g}{dt} = \frac{N_e}{\tau_{eg}}\left(1 - \frac{N_g}{N_{DG}}\right) - \frac{N_g}{\tau_{ge}}\left(1 - \frac{N_e}{N_{DE}}\right) - \frac{N_g}{\tau_{gr}} - \Gamma v_g \frac{g_G}{1 + \varepsilon S_{ave}} S_{ave}. \tag{4}$$

Equations (1)–(4) describe the changes of carrier densities in SCH (N_s), in WL (N_w), in ES (N_e), and in GS (N_g), respectively. N_{DE} and N_{DG} are the volume density of states of ES and GS, and $N_{DE} = 4N_D$ and $N_{DG} = 2N_D$, 4 and 2 are the number of degeneracy of ES and GS including the spin [19,22], N_D is the quantum dot volume density. Γ is the optical confinement factor, v_g is the group velocity of light in the active region, ε is the gain compression factor, S_{ave} is the average photon density over the QD-SOA cavity length which can be achieved by

$$S_{ave} = \frac{1}{L}\int_0^L S(z)dz, \tag{5}$$

where L is the length of QD-SOA, z is the distance in longitudinal direction ($z = 0$ and $z = L$ stand for input facet and output facet of QD-SOA, respectively). The relationship between photon density and light power is

$$S = \frac{\lambda P}{\eta_c A h c v_g}, \tag{6}$$

where η_c is the differential quantum efficiency and A is the cross sectional area of active region, λ is the input light wavelength. If we consider QD-SOA as a lumped element and assume that the carrier density distributions of all states approximate constants in the length direction [5,6,15,18], the optical propagation equation can be described as

$$P(z) = \exp((\Gamma g - \alpha)z)P(0), \tag{7}$$

where α is the internal loss, $P(0)$ is the input photon density, g is calculated as the sum of contributions from the linear optical gains of ES (g_E) and GS (g_G) with a form given by Refs. [10,19]. The average photon density in Eq. (5) can be obtained by substituting Eqs. (6) and (7) into Eq. (5), as

$$S_{ave} = \frac{\lambda P(0)[\exp((\Gamma g - \alpha)L) - 1]}{\eta_c A h c v_g (\Gamma g - \alpha)L}. \tag{8}$$

In our model, we neglect the inhomogeneous broadening inherited from the nonuniform distribution of QD size and the propagation of amplified spontaneous emission for the purpose of simulation efficiency [5–7,21].

2.2 Circuit model of QD-SOA

In order to eliminate the nonphysical solutions when solving the standard rate equations in steady-state conditions [13], we develop a new circuit model of QD-SOA through suitable algebraic manipulations of the rate equations, which makes our solutions insensitive to the initial values of the carrier densities:

$$N_\beta = N_{\beta 0}\exp\left(\frac{qV_\beta}{nKT}\right), \tag{9}$$

$$P = V_p^2/R_p, \tag{10}$$

where $N_{\beta 0}$ and V_β (β = s, w, e, g) are the equilibrium carrier densities and the equivalent diode voltages in SCH, WL, ES and GS, respectively, n is diode ideality factor (set equal to two) [16], K is Boltzmann's constant, T is QD-SOA's temperature, P is the light power, V_p and R_p (set as 1 Ω) are equivalent voltage and resistor of light. Substituting Eq. (9) into Eq. (1), and through appropriate manipulations, we can get the equivalent circuit model of SCH, as shown in Fig. 2(a), in which

$$I_{DS1} = \frac{qVN_{s0}}{2\tau_{sw}}\left[\exp\left(\frac{qV_s}{nKT}\right) - 1 + \frac{2q\tau_{sw}}{nKT}\exp\left(\frac{qV_s}{nKT}\right)\frac{dV_s}{dt}\right], \tag{11}$$

$$I_{\mathrm{CS1}} = \frac{qVN_{\mathrm{s0}}}{2\tau_{\mathrm{sw}}}, \tag{12}$$

$$I_{\mathrm{DS2}} = \frac{qVN_{\mathrm{s0}}}{2\tau_{\mathrm{sw}}}\left[\exp\left(\frac{qV_{\mathrm{s}}}{nKT}\right)-1\right], \tag{13}$$

$$I_{\mathrm{CS2}} = \frac{qVN_{\mathrm{s0}}}{2\tau_{\mathrm{sw}}}, \tag{14}$$

$$I_{\mathrm{DS3}} = \frac{qVN_{\mathrm{s0}}}{\tau_{\mathrm{sr}}}\left[\exp\left(\frac{qV_{\mathrm{s}}}{nKT}\right)-1\right], \tag{15}$$

$$I_{\mathrm{CS3}} = \frac{qVN_{\mathrm{s0}}}{\tau_{\mathrm{sr}}}, \tag{16}$$

$$I_{\mathrm{TS1}} = I_{\mathrm{DW2}} + I_{\mathrm{CW2}}. \tag{17}$$

Substituting Eq. (9) into Eq. (2), we can get the equivalent circuit model of WL, as shown in Fig. 2(b), in which

$$I_{\mathrm{DW1}} = \frac{qVN_{\mathrm{w0}}}{\tau_{\mathrm{wr}}}\left[\exp\left(\frac{qV_{\mathrm{w}}}{nKT}\right)-1+\frac{q\tau_{\mathrm{wr}}}{nKT}\exp\left(\frac{qV_{\mathrm{w}}}{nKT}\right)\frac{\mathrm{d}V_{\mathrm{w}}}{\mathrm{d}t}\right], \tag{18}$$

$$I_{\mathrm{CW1}} = \frac{qVN_{\mathrm{w0}}}{\tau_{\mathrm{wr}}}, \tag{19}$$

$$I_{\mathrm{DW2}} = \frac{qVN_{\mathrm{w0}}}{\tau_{\mathrm{ws}}}\left[\exp\left(\frac{qV_{\mathrm{w}}}{nKT}\right)-1\right], \tag{20}$$

$$I_{\mathrm{CW2}} = \frac{qVN_{\mathrm{w0}}}{\tau_{\mathrm{ws}}}, \tag{21}$$

$$I_{\mathrm{DW3}} = \frac{qVN_{\mathrm{w0}}}{\tau_{\mathrm{we}}}\left[\exp\left(\frac{qV_{\mathrm{w}}}{nKT}\right)-1\right], \tag{22}$$

$$I_{\mathrm{CW3}} = \frac{qVN_{\mathrm{w0}}}{\tau_{\mathrm{we}}}, \tag{23}$$

$$I_{\mathrm{TW1}} = 2(I_{\mathrm{DS2}} + I_{\mathrm{CS2}}), \tag{24}$$

$$I_{\mathrm{TW2}} = I_{\mathrm{DDE2}} + I_{\mathrm{CDE2}}, \tag{25}$$

$$I_{\mathrm{TW3}} = I_{\mathrm{SDE4}}. \tag{26}$$

Substituting Eq. (9) into Eq. (3), we can get the equivalent circuit model of ES, as shown in Fig. 2(c), in which

$$I_{\mathrm{DDE1}} = \frac{qVN_{\mathrm{e0}}}{\tau_{\mathrm{er}}}\left[\exp\left(\frac{qV_{\mathrm{e}}}{nKT}\right)-1+\frac{q\tau_{\mathrm{er}}}{nKT}\exp\left(\frac{qV_{\mathrm{e}}}{nKT}\right)\frac{\mathrm{d}V_{\mathrm{e}}}{\mathrm{d}t}\right], \tag{27}$$

$$I_{\mathrm{CDE1}} = \frac{qVN_{\mathrm{e0}}}{\tau_{\mathrm{er}}}, \tag{28}$$

$$I_{\mathrm{DDE2}} = \frac{qVN_{\mathrm{e0}}}{\tau_{\mathrm{ew}}}\left[\exp\left(\frac{qV_{\mathrm{e}}}{nKT}\right)-1\right], \tag{29}$$

$$I_{\mathrm{CDE2}} = \frac{qVN_{\mathrm{e0}}}{\tau_{\mathrm{ew}}}, \tag{30}$$

$$I_{\mathrm{DDE3}} = \frac{qVN_{\mathrm{e0}}}{\tau_{\mathrm{eg}}}\left[\exp\left(\frac{qV_{\mathrm{e}}}{nKT}\right)-1\right], \tag{31}$$

$$I_{\mathrm{CDE3}} = \frac{qVN_{\mathrm{e0}}}{\tau_{\mathrm{eg}}}, \tag{32}$$

$$I_{\mathrm{SDE4}} = \frac{\tau_{\mathrm{ew}}\tau_{\mathrm{ws}}}{4qV\tau_{\mathrm{we}}N_{\mathrm{D}}}(I_{\mathrm{DDE2}} + I_{\mathrm{CDE2}})(I_{\mathrm{DW2}} + I_{\mathrm{CW2}}), \tag{33}$$

$$I_{\mathrm{SDE5}} = \frac{\tau_{\mathrm{ew}}}{4qVN_{\mathrm{D}}}(I_{\mathrm{DDE2}} + I_{\mathrm{CDE2}})(I_{\mathrm{DDG2}} + I_{\mathrm{CDG2}}), \tag{34}$$

$$I_{\mathrm{TDE1}} = I_{\mathrm{DW3}} + I_{\mathrm{CW3}}, \tag{35}$$

$$I_{\mathrm{TDE2}} = I_{\mathrm{DDG2}} + I_{\mathrm{CDG2}}, \tag{36}$$

$$I_{\mathrm{TDE3}} = I_{\mathrm{SDG3}}, \tag{37}$$

$$G_{\mathrm{SE1}} = \frac{\lambda\Gamma qVg_{\mathrm{E}}}{\eta_c Ahc(1+\varepsilon S_{\mathrm{ave}})}V_p^2. \tag{38}$$

Substituting Eqs. (6) and (9) into Eq. (4), we can get the equivalent circuit model of GS, as shown in Fig. 2(d), in which

$$I_{\mathrm{DDG1}} = \frac{qVN_{\mathrm{g0}}}{\tau_{\mathrm{gr}}}\left[\exp\left(\frac{qV_{\mathrm{g}}}{nKT}\right)-1+\frac{q\tau_{\mathrm{gr}}}{nKT}\exp\left(\frac{qV_{\mathrm{g}}}{nKT}\right)\frac{\mathrm{d}V_{\mathrm{g}}}{\mathrm{d}t}\right], \tag{39}$$

$$I_{\mathrm{CDG1}} = \frac{qVN_{\mathrm{g0}}}{\tau_{\mathrm{gr}}}, \tag{40}$$

$$I_{\mathrm{DDG2}} = \frac{qVN_{\mathrm{g0}}}{\tau_{\mathrm{ge}}}\left[\exp\left(\frac{qV_{\mathrm{g}}}{nKT}\right)-1\right], \tag{41}$$

$$I_{\mathrm{CDG2}} = \frac{qVN_{\mathrm{g0}}}{\tau_{\mathrm{ge}}}, \tag{42}$$

$$I_{\mathrm{SDG3}} = \frac{\tau_{\mathrm{ew}}\tau_{\mathrm{ge}}}{2qV\tau_{\mathrm{eg}}N_{\mathrm{D}}}(I_{\mathrm{DDE2}} + I_{\mathrm{CDE2}})(I_{\mathrm{DDG2}} + I_{\mathrm{CDG2}}), \tag{43}$$

$$I_{\mathrm{TDG1}} = I_{\mathrm{DDE3}} + I_{\mathrm{CDE3}}, \tag{44}$$

$$I_{\mathrm{TDG2}} = I_{\mathrm{SDE5}}, \tag{45}$$

$$G_{\mathrm{SG1}} = \frac{\lambda \Gamma q V g_{\mathrm{G}}}{\eta_c A h c (1 + \varepsilon S_{\mathrm{ave}})} V_p^2. \tag{46}$$

The optical propagation Eq. (7) can be equalized as the model shown in Fig. 2(e).

Utilizing PSPICE sub-circuits, the above equations can be mapped directly into the circuits shown in Fig. 2. The typical parameters used in the simulation are listed in Table 1.

The optical gain of QD-SOA versus injection current is shown in Fig. 3. It has a GS peak at 1554 nm (0.8 eV), and an ES peak at 1413 nm (0.88 eV). We can find that the optical gain increases as the injection current is increased. The optical gain is GS-dominant at low current, and it shifts to ES-dominant when the injection current increases beyond 60 mA. In order to verify the validity of our model, we first study the QD-SOA saturation property. The wavelength of input light is 1550 nm. It can be shown as expected in Fig. 4 that with increasing injection current, the output power tends to be constant. Since the emission of ES is negligible at this wavelength, it is mainly because that when the injection current becomes high enough, the state of GS is almost occupied completely by the carriers ($N_{\mathrm{g}} \approx N_{\mathrm{DG}}$).

Figure 5 illustrates the saturation curves of QD-SOA for various injection currents. It can be obviously seen that as the input optical power increases, the optical gain starts to saturate due to larger consumption of carriers, and if given sufficient injection current (exceeds 20 mA), higher biased currents in QD-SOA just leads to higher saturation powers but not higher small-signal gain values due to the limited state densities. These saturation characteristics obtained by PSPICE based simulation exhibit a similar evolution trend as the work reported in Ref. [9].

Next, we analyze the QD-SOA dynamic performance. A series of square-shaped pulses modulated at 20 Gbit/s with pulse width of 20 ps is injected into QD-SOA. As we know, the change of carrier density affects not only the optical gain but also the refractive index, which results in the phase fluctuation of the light. The optical gain and phase dynamics are linked by the Kramers-Kronig relations, and the chirp of the light can be obtained by $\Delta\nu = \frac{\alpha_{\mathrm{L}} L}{4\pi} \frac{\partial g}{\partial t}$ [5], where α_{L} is the linewidth enhancement

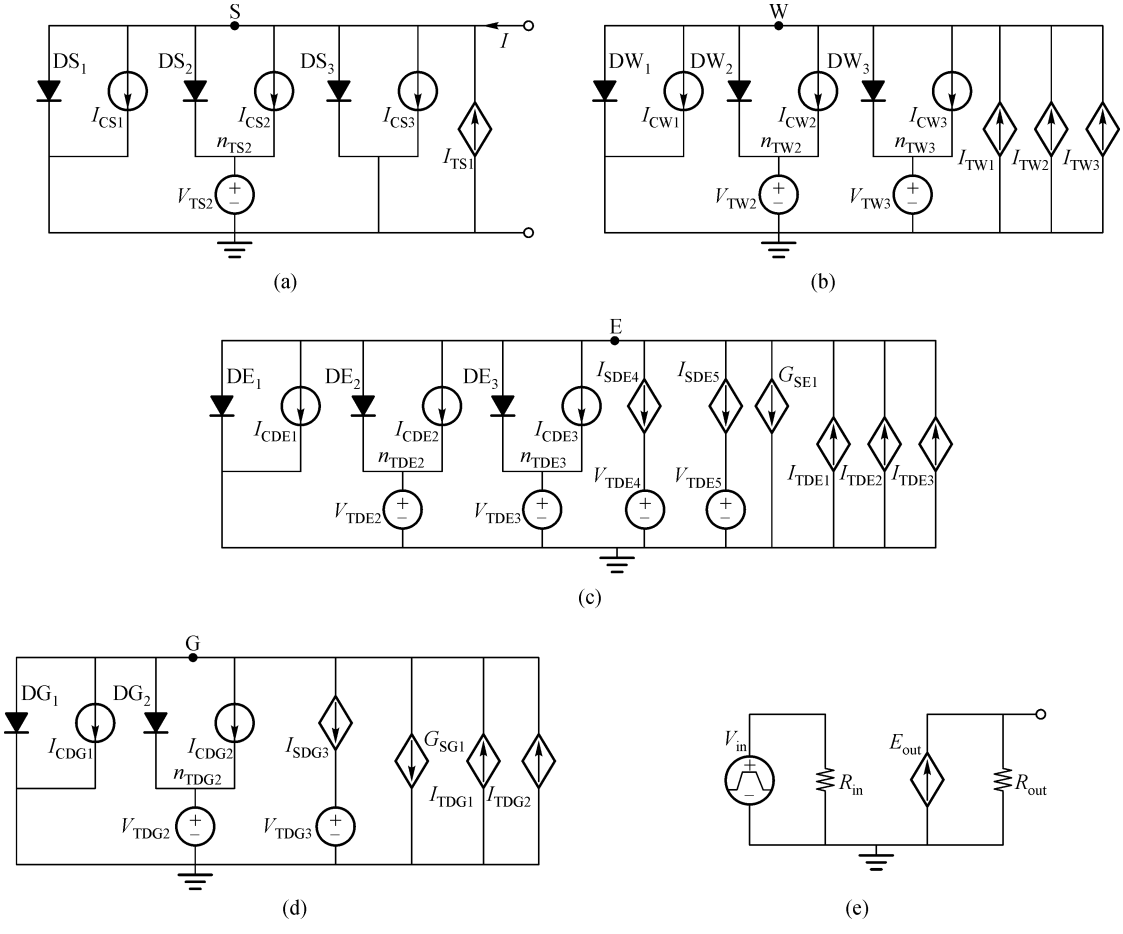


Fig. 2 Equivalent sub-circuits of QD-SOA. (a) SCH; (b) WL; (c) ES; (d) GS; (e) optical propagation circuit

Table 1 Parameter values used in PSPICE simulation

parameter	value	parameter	value
QD volume density (N_D)	6×10^{22} m^{-3} [19]	carrier relaxation time from WL to ES (τ_{we})	1 ps [19]
SOA length (L)	900 μm [19]	carrier escape time from ES to WL (τ_{ew})	0.2 ns
active region volume (V)	6×10^{-16} m^3	carrier relaxation time from ES to GS (τ_{eg})	0.3 ps
active region cross sectional area (A)	6×10^{-13} m^2	carrier escape time from GS to ES (τ_{ge})	0.2 ns [19]
internal loss (α)	100 m^{-1} [19]	recombination life time in SCH (τ_{sr})	4.5 ns [19]
nonlinear gain coefficient (ε)	1.045×10^{-22} m^3 [19]	recombination life time in WL (τ_{wr})	3 ns [17]
GS band gap (E_{gcv})	0.8 eV [17]	recombination life time in ES (τ_{er})	2.8 ns [17]
homogeneous line broadening ($\hbar\Gamma_{cv}$)	20 meV [17]	recombination life time in GS (τ_{gr})	2.8 ns [17]
optical confinement factor (Γ)	0.06 [17]	differential quantum efficiency (η_c)	0.45 [17]

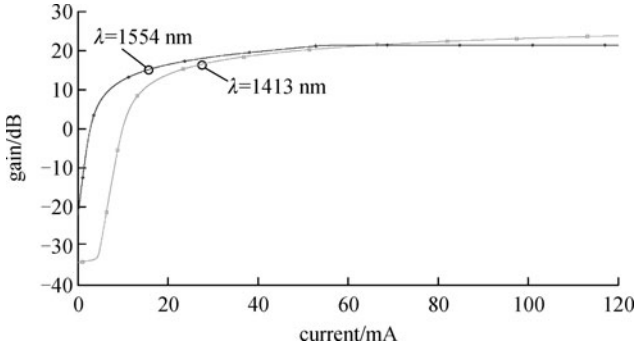


Fig. 3 Optical gain of QD-SOA versus injection current for various wavelengths of input light (input optical power is P_{in}= 0.1 mW)

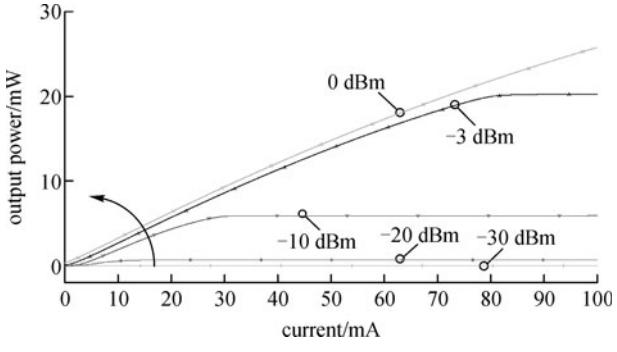


Fig. 4 Optical output power of QD-SOA as a function of injection current for different input optical powers

factor (LEF). The subcircuit for the output chirp of QD-SOA is given in Fig. 6, in which

$$E_g = g,$$

$$C_v = \frac{\alpha_L L}{4\pi},$$

$$\Delta v = E_{chi} = -I_{c_v}.$$

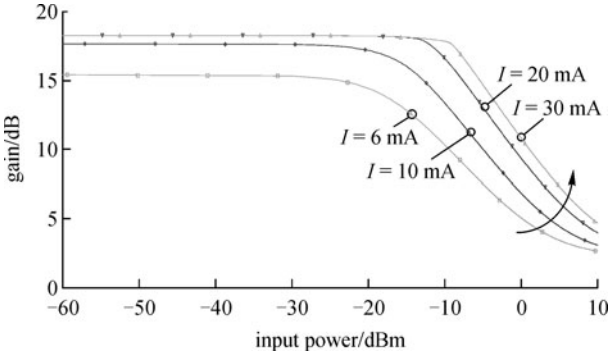


Fig. 5 Optical gain of QD-SOA as a function of input optical power for different injection current

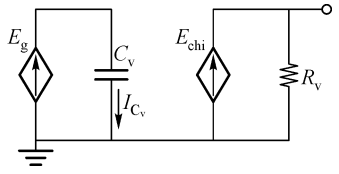


Fig. 6 Subcircuit for output chirp of QD-SOA

The output power and associated chirp are shown in Fig. 7 with I = 35 mA. For Figs. 7(a), 7(b), the input power P_{in} is 0.1 mW, and for Figs. 7(c), 7(d), the input power P_{in} is 1 mW. It can be found that when the input power is increased to the saturation region, strong overshoot near the leading edge of each output pulse becomes pronounced and the output chirp becomes relatively large and asymmetric due to the larger carrier consumption and the finite gain recovery time. This variation of the optical output power and chirp is similar with the previous works in Ref. [6].

3 Cross gain wavelength conversion based on QD-SOA circuit model

SOA-based all-optical signal processing has attracted much attention for its superior performance over the past

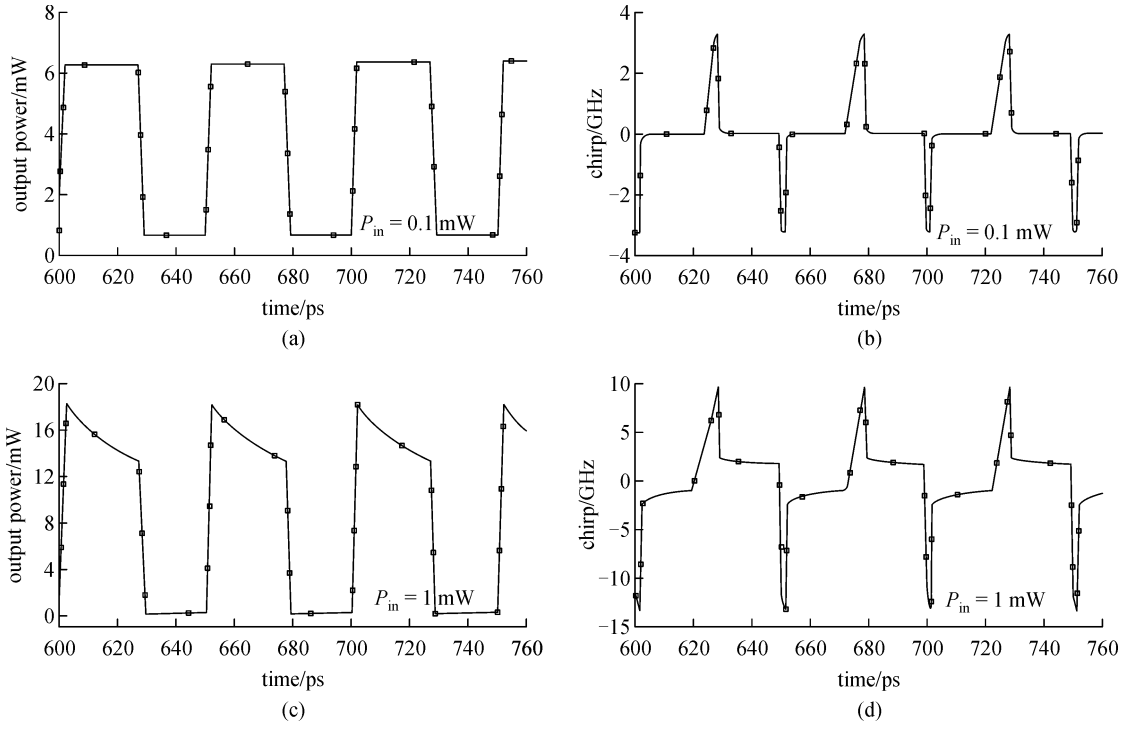


Fig. 7 Power and chirp of output light with bit-rate of 20 Gbit/s, $\alpha_L = 0.1$, $I = 35$ mW. (a) Output power of light for $P_{in} = 0.1$ mW; (b) output chirp of light for $P_{in} = 0.1$ mW; (c) output power of light for $P_{in} = 1$ mW; (d) output chirp of light for $P_{in} = 1$ mW

decade [23]. Cross-grain (XG) wavelength converters, which are an essential component in wavelength-division multiplexed systems and photonic networks, are very simple to realize and have shown impressive performance in QD, QW and bulk SOAs. In this paper, we use PSPICE circuit model of QD-SOA to investigate wavelength conversion at 1550 nm.

A series of signal lightwave (SW) of 1546 nm is modulated at 40 Gbit/s with ultra short pulses (2 ps), and the wavelength of continuous probe lightwave (CW) is 1550 nm. Both the SW and CW are simultaneously injected into QD-SOA to perform wavelength conversion based on XGM. The input peak power of SW P_{sw} is 5 mW, the input power of PW P_{pw} is 0.01 mW. In the presence of the probe lightwave, the Eqs. (3) and (4) should be modified as

$$\begin{aligned}\frac{\mathrm{d}N_e}{\mathrm{d}t} =& \frac{N_w}{\tau_{we}}\left(1-\frac{N_e}{N_{DE}}\right)-\frac{N_e}{\tau_{ew}}+\frac{N_g}{\tau_{ge}}\left(1-\frac{N_e}{N_{DE}}\right)\\ &-\frac{N_e}{\tau_{eg}}\left(1-\frac{N_g}{N_{DG}}\right)-\frac{N_e}{\tau_{er}}-\Gamma v_g\frac{g_{ESW}}{1+\varepsilon S_{sw}}S_{sw}\\ &-\Gamma v_g\frac{g_{ECW}}{1+\varepsilon S_{cw}}S_{cw},\end{aligned} \tag{47}$$

$$\begin{aligned}\frac{\mathrm{d}N_g}{\mathrm{d}t} =& \frac{N_e}{\tau_{eg}}\left(1-\frac{N_g}{N_{DG}}\right)-\frac{N_g}{\tau_{ge}}\left(1-\frac{N_e}{N_{DE}}\right)\\ &-\frac{N_g}{\tau_{gr}}-\Gamma v_g\frac{g_{GSW}}{1+\varepsilon S_{sw}}S_{sw}-\Gamma v_g\frac{g_{GCW}}{1+\varepsilon S_{cw}}S_{cw},\end{aligned} \tag{48}$$

where S_{sw} represents the average photon density of SW, and S_{cw} represents the average photon density of CW along the length direction. g_{ESW} and g_{GSW} are the linear optical gains of SW from ES and GS, g_{ECW} and g_{GCW} are the linear optical gains of CW from ES and GS.

In this case, a voltage-controlled current source G_{SE2} and G_{SG2} should be added in ES and GS sub-circuits, respectively shown in Fig. 8, in which

$$G_{SE2} = \frac{\lambda_{cw}\Gamma q V g_{ECW}}{\eta_c A h c(1+\varepsilon S_{cw})}V_{cw}^2,$$

$$G_{SG2} = \frac{\lambda_{cw}\Gamma q V g_{GCW}}{\eta_c A h c(1+\varepsilon S_{cw})}V_{cw}^2,$$

where λ_{cw} and V_{cw} are the wavelength and equivalent voltage of the continuous probe light.

Figure 9 shows the normalized intensity of input SW and output converted CW. It can be seen that the power of CW decreases while the power of SW increases which is ascribed to the carrier depletion in QD-SOA. With the same TE polarized SW and CW injected into the QD-SOA, a conjugate signal will be generated by four wave mixing (FWM). In our simulation, the effect of FWM on the XGM efficiency was neglected.

Figure 10 shows the calculated normalized small signal XGM responses dependent on the SW-CW detuning when the injection current is 30 and 200 mA, the detunings between SW and CW are -2 nm, -10 nm and -20 nm,

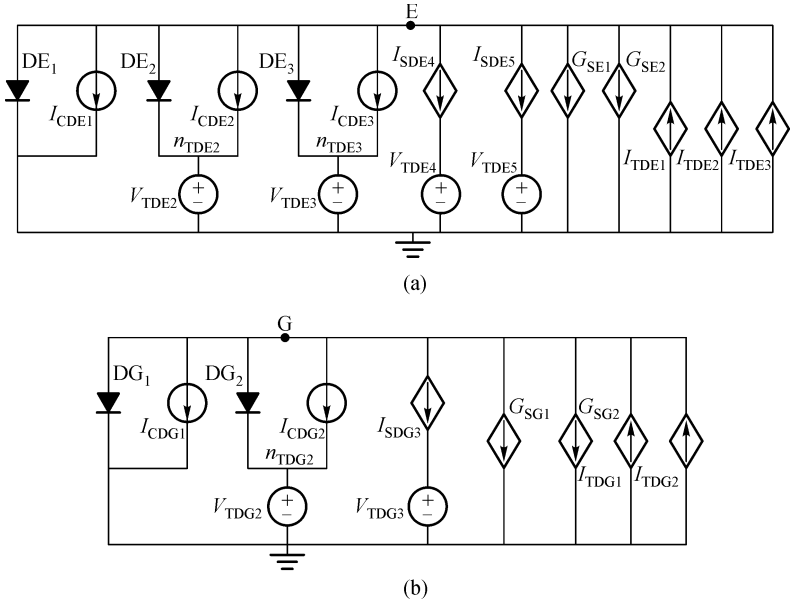


Fig. 8 Modified subcircuits. (a) ES of QD-SOA; (b) GS of QD-SOA

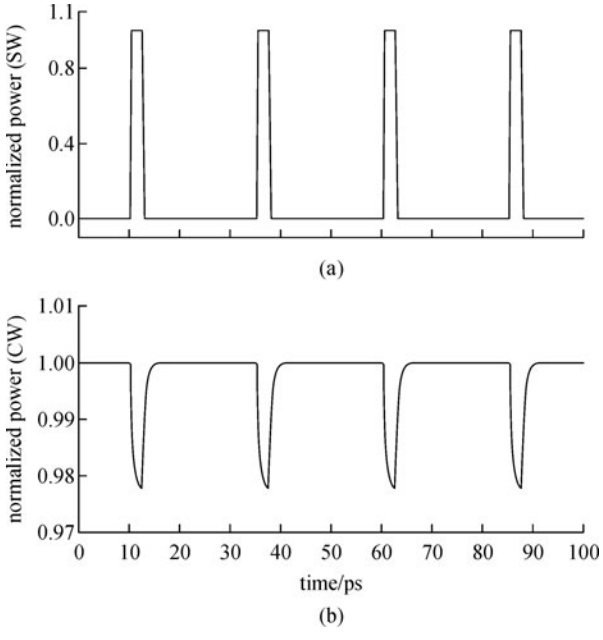


Fig. 9 Normalized power of signal with $I = 40$ mA. (a) Normalized intensity of input SW; (b) normalized intensity of output CW

respectively. The input SW is sinusoidally modulated with the average power of 5 mW and CW with the power of 0.01 mW. In Fig. 10 the calculated small signal XGM continues to decrease as the modulation frequency increases. When the current injection is low (30 mA), most of QD carrier reservoirs are depleted and cannot directly supply an empty QD GS with carrier through ultra fast QD carrier relaxation. Thus, at high current injection (200 mA), most of the QD carrier reservoirs are occupied and the ultra fast XGM due to spectral hole burning (SHB) becomes dominant which makes the XGM response less dependable of the modulation frequency [24]. These simulations are in good agreement with the work in Ref. [25].

4 Conclusions

We have proposed an equivalent circuit model of QD-SOA by employing the standard rate equations. Utilizing the model, saturation property and dynamic performance of QD-SOA have been analyzed with the aid of PSPICE circuit simulator. Furthermore, XGM wavelength conversion has been investigated based on our QD-SOA circuit model, and the results show that by increasing the injection current, SHB becomes the dominant XGM mechanism that enhances the QD-SOA XGM responses. Considering the simplicity and the advantages of the circuit simulator in integrated fields such as its high simulation efficiency, the circuit models can be extended to be used for various optoelectronics system designs including QD-SOA and other optical devices such as multiplexers, interferometers and modulators, etc., and utilizing existing PSPICE-analysis operations, it can be also used directly for the implementations of various system analysis such as Fourier analysis, Monte Carlo analysis and minimum error analysis. Therefore, it can be expected that there is a great potential value of circuit modeling for large scale optical integration.

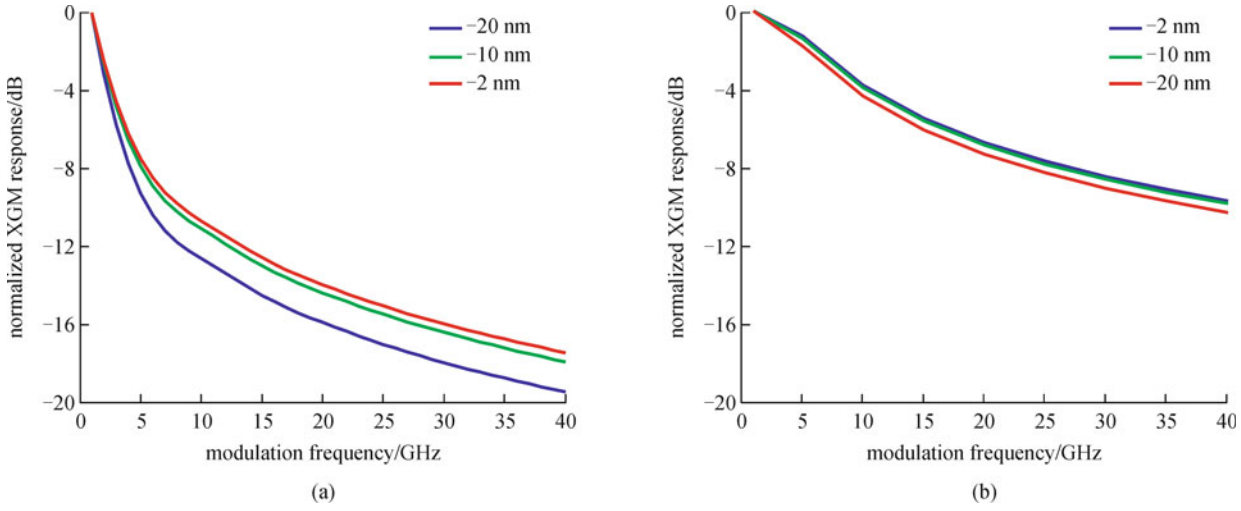


Fig. 10 Normalized small signal XGM responses at different SW-CW detuning. (a) Injection current is 30 mA; (b) injection current is 200 mA

Acknowledgements This work was supported by the National High Technology Research and Development Program of China (No. 2007AA03Z414) and the National Natural Science Foundation of China (Grant Nos. 60877056 and 60777019).

References

1. Asada M, Miyamoto Y, Suematsu Y. Gain and the threshold of three-dimensional quantum-box lasers. IEEE Journal of Quantum Electronics, 1986, QE-22(9): 1915–1921
2. Willatzen M, Tanaka T, Arakawa Y, Singh J. Polarization dependence of optoelectronic properties in quantum dots and quantum wires-consequences of valence-band mixing. IEEE Journal of Quantum Electronics, 1994, 30(3): 640–653
3. Bhattacharya P. Self-organized quantum dots. Journal of Physics D, 2005, 38(13): 2055–2150
4. Huang X, Stintz A, Li H, Lester L F, Cheng J, Malloy K J. Passive mode-locking in 1.3 μm two-section InAs quantum dot lasers. Applied Physics Letters, 2001, 78(19): 2825–2827
5. Ben-Ezra Y, Haridim M, Lembrikov B I. Theoretical analysis of gain-recovery time and chirp in QD-SOA. IEEE Photonics Technology Letters, 2005, 17(19): 1803–1805
6. Li X X, Li G F. Comments on "theoretical analysis of gain-recovery time and chirp in QD-SOA". IEEE Photonics Technology Letters, 2006, 18(22): 2434–2435
7. Huang L R, Yu Y, Tian P, Huang D X. Polarization-insensitive quantum-dot coupled quantum-well semiconductor optical amplifier. Semiconductor Science and Technology, 2009, 24(1): 1–7
8. Li X X, Li G F. Static gain, optical modulation response, and nonlinear phase noise in saturated quantum-dot semiconductor optical amplifiers. IEEE Journal of Quantum Electronics, 2009, 45 (5): 499–505
9. Uskov A V, O'Reilly E P, Laemmlin M, Ledentsov N N, Bimberg D. On gain saturation in quantum dot semiconductor optical amplifiers. Optics Communications, 2005, 248(1–3): 211–219
10. Sugawara M, Mukai K, Nakata Y, Ishikawa H, Sakamoto A. Effect of homogeneous broadening of optical gain on lasing spectra in self-assembled $In_xGa_{1-x}As/GaAs$ quantum dot lasers. Physical Review B: Condensed Matter and Materials Physics, 2001, 61(11): 7595–7603
11. Manning R J, Ellis A D, Poustie A J, Blow K J. Semiconductor laser amplifiers for ultrafast all-optical signal processing. Journal of the Optical Society of America B: Optical Physics, 1997, 14(11): 3204–3216
12. Cotter D, Manning R J, Blow K J, Ellis A D, Kelly A E, Nesset D, Phillips I D, Poustie A J, Rogers D C. Nonlinear optics for high speed digital information processing. Science, 1999, 286(5444): 1523–1528
13. Mena P V, Kang S M, Temple T A D. Rate-equation-based laser models with a single solution regime. Journal of Lightwave Technology, 1997, 15(4): 717–730
14. Mena P V. Circuit-level modeling and simulation of semiconductor lasers. Dissertation for the Doctoral Degree, University of Illinois at Chicago, 1998
15. Jou J J, Liu C K, Lee S L. A unified circuit model for static and dynamic analyses of semiconductor optical amplifiers and laser diodes. Solid-State Electronics, 2007, 51(3): 360–365
16. Lu M F, Deng J S, Juang C, Jou M J, Lee B J. Equivalent circuit model of quantum well lasers. IEEE Journal of Quantum Electronics, 1995, 31(8): 418–1422
17. Yavari M H, Ahmadi V. Circuit-level implementation of semiconductor self-assembled quantum dot laser. IEEE Journal on Selected Topics in Quantum Electronics, 2009, 15(3): 774–779
18. Maram R, Baghban H, Rasooli H, Ghorbani R, Rostami A. Equivalent circuit model of quantum dot semiconductor optical amplifiers: dynamic behaviour and saturation properties. Journal of Optics A: Pure and Applied Optics, 2009, 11(10): 105205
19. Gioannini M, Montrosset I. Numerical analysis of the frequency chirp in quantum-dot semiconductor lasers. IEEE Journal of Quantum Electronics, 2007, 43(10): 941–949

20. Berg T W, Bischoff S, Magnusdottir I, Mork J. Ultrafast gain recovery and modulation limitations in self-assembled quantum-dot devices. IEEE Photonics Technology Letters, 2001, 13(6): 541–543
21. Ben-Ezra Y, Lembrikov B I, Haridim M. Acceleration of gain recovery and dynamics of electrons in QD-SOA. IEEE Journal of Quantum Electronics, 2005, 41(10): 1268–1273
22. Kim J, Kondratko P K, Chuang S L, Walter G, Holonyak N, Heller R D, Zhang X B, Dupuis R D. Tunneling injection quantum-dot lasers with polarization-dependent photon-mediated carrier redistribution and gain narrowing. IEEE Journal of Quantum Electronics, 2005, 41(11): 1369–1379
23. Houbavlis T, Zoiros K E, Kalyvas M, Theophilopoulos G, Bintjas C, Yiannopoulos K, Pleros N, Vlachos K, Avramopoulos H, Schares L, Occhi L, Guekos G, Taylor J R, Hansmann S, Miller W. All-optical signal processing and applications within the esprit project DO_ALL. Journal of Lightwave Technology, 2005, 23(2): 781–801
24. Uskov A V, Mork J, Tromborg B, Berg T W, Magnusdottir I, O'Reilly E P. On high-speed cross-gain modulation without pattern effects in quantum dot semiconductor optical amplifiers. Optics Communications, 2003, 227(4–5): 363–369
25. Kim J, Laemmlin M, Meuer C, Bimberg D, Eisenstein G. Theoretical and experimental study of high-speed small-signal cross-gain modulation of quantum-dot semiconductor optical amplifiers. IEEE Journal of Quantum Electronics, 2009, 45(3): 240–248